Cell Reports, Volume *32*

Supplemental Information

Distinct Mechanisms of Over-Representation of Landmarks and Rewards in the Hippocampus

Masaaki Sato, Kotaro Mizuta, Tanvir Islam, Masako Kawano, Yukiko Sekine, Takashi Takekawa, Daniel Gomez-Dominguez, Alexander Schmidt, Fred Wolf, Karam Kim, Hiroshi Yamakawa, Masamichi Ohkura, Min Goo Lee, Tomoki Fukai, Junichi Nakai, and Yasunori Hayashi

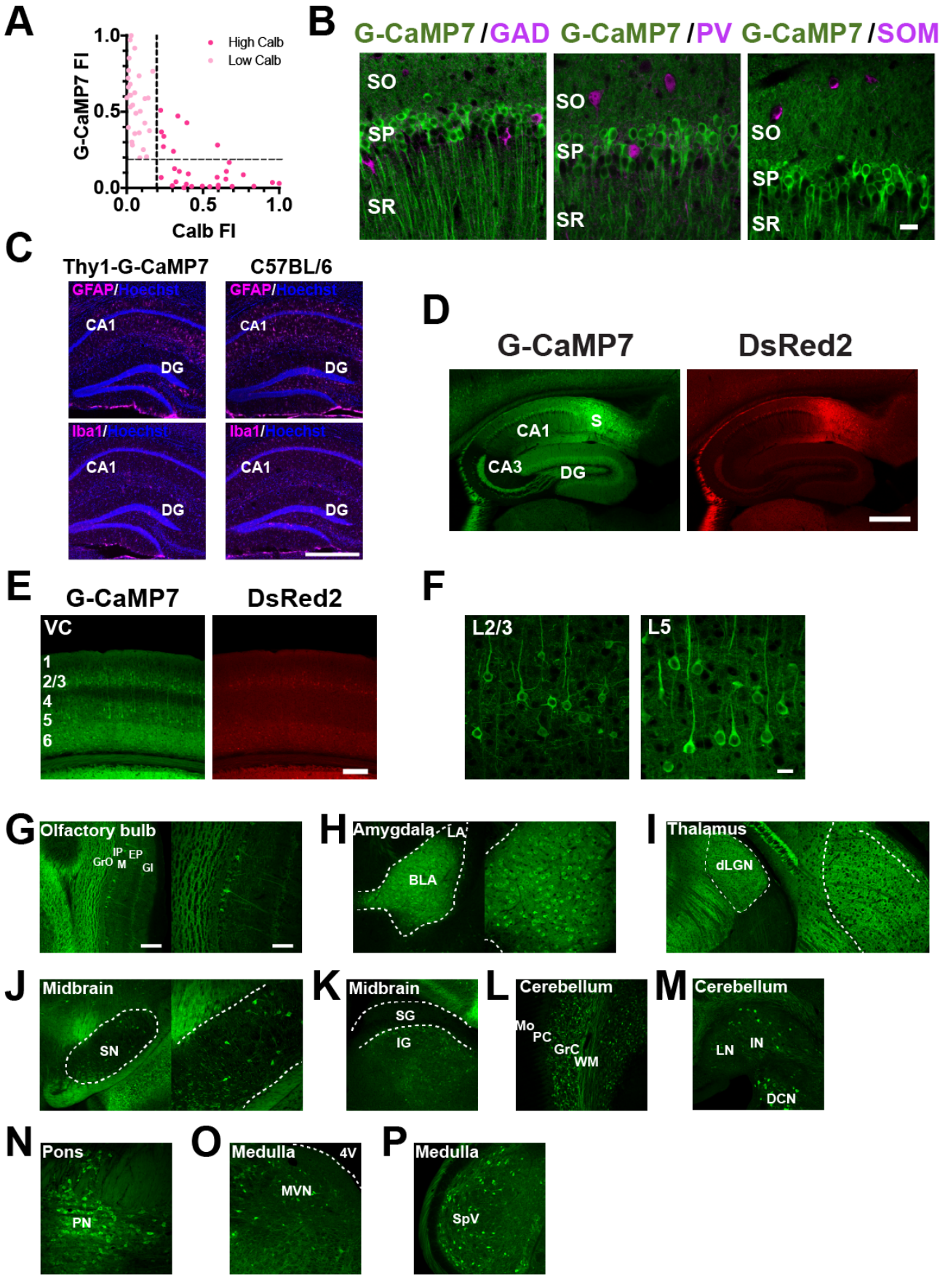
A
1.0
0.5
0.0
0.0
0.5
1.0
G-CaMP7 FI
Calb FI
High Calb
Low Calb
B
G-CaMP7 /GAD G-CaMP7 /PV G-CaMP7 /SOM
SO
SP
SR
C
Thy1-G-CaMP7
C57BL/6
GFAP/Hoechst
Iba1/Hoechst
CA1
DG
D
G-CaMP7
DsRed2
CA1
S
CA3
DG
E
G-CaMP7
DsRed2
VC
1
2/3
4
5
6
F
L2/3
L5
G
Olfactory bulb
GrO
IP
M
EP
Gl
H
Amygdala
LA
BLA
I
Thalamus
dLGN
J
Midbrain
SN
K
Midbrain
SG
IG
L
Cerebellum
Mo
PC
GrC
WM
M
Cerebellum
LN
IN
DCN
N
Pons
PN
O
Medulla
4V
MVN
P
Medulla
SpV

Figure S1. Transgene expression in Thy1-G-CaMP7 transgenic mice. Related to Figure 1 and STAR Methods. (A) A scatter plot showing normalized fluorescence intensities (FIs) of G-CaMP7 expression and calbindin D-28K (Calb) immunolabeling (n = 60 cells from 2 mice). The broken lines indicate the threshold (FI = 0.2) that divides high and low expression levels. Cells with high and low calbindin expression levels are indicated in magenta and pink, respectively (normalized G-CaMP7 fluorescence, 0.56 ± 0.22 in low-calbindin cells [0 ≦ normalized calbindin fluorescence < 0.2] vs. 0.13 ± 0.15 in high-calbindin cells [0.2 ≦ normalized calbindin fluorescence ≦ 1], mean ± SD, $P < 0.0001$, $t_{(58)} = 8.72$; unpaired two-tailed t-test, n = 30 cells each from 2 mice), (B) G-CaMP7 expression (green) overlaid with glutamic acid decarboxylase 65/67 (GAD, left), parvalbumin (PV, middle) or somatostatin (SOM, right) immunofluorescence (magenta) in the dorsal hippocampal CA1 area at 4 months of age. SO, stratum oriens; SP, stratum pyramidale; SR, stratum radiatum. Scale bar = 20 μm. (C) GFAP (top) or Iba1 (bottom) immunofluorescence (magenta) in the hippocampus of Thy1-G-CaMP7 (left) and C57BL/6 (right) mice overlaid with Hoechst nuclear counterstaining (blue). DG, dentate gyrus; CA1, CA1 area of the hippocampus. Scale bar = 500 μm. (D) Expression of G-CaMP7 (left) and DsRed2 (right) in a parasagittal section of the hippocampus at 1 month of age. CA3, CA3 area of the hippocampus; S, subiculum. Scale bar = 500 μm. (E) Low-magnification images of G-CaMP7 (left) and DsRed2 (right) expression in the visual cortex (VC) at 3 months of age. Scale bar = 200 μm. (F) High-magnification images of G-CaMP7 expression in layer 2/3 (L2/3, left) and layer 5 (L5, right) of the VC at 3 months of age. Scale bar = 20 μm. (G-P) G-CaMP7 expression at 1 month of age in the olfactory bulb (G), amygdala (H), thalamus (I), midbrain (J, K), cerebellum (L, M), pons (N) and medulla (O, P). EP, external plexiform layer; GI, glomerular layer; GrO, granule cell layer of the olfactory bulb; IP, internal plexiform layer; M, mitral cell layer; BLA, basolateral amygdala; LA, lateral amygdala; dLGN; dorsal lateral geniculate nucleus; SN, substantia nigra; IG, intermediate gray layer of the superior colliculus; SG; superficial gray layer of the superior colliculus; GrC, granule cell layer of the cerebellum; Mo, molecular layer; PC, Purkinje cell layer; WM, white matter; DCN, dorsal cochlear nucleus; IN, interposed cerebellar nucleus; LN, lateral cerebellar nucleus; PN, pontine nucleus; MVN, medial vestibular nucleus; 4V, fourth ventricle; SpV, spinal trigeminal nucleus. Scale bar = 200 μm (left panels of G, H, I and J as well as K, N, O and P) or 100 μm (right panels of G, H, I and J as well as L and M).

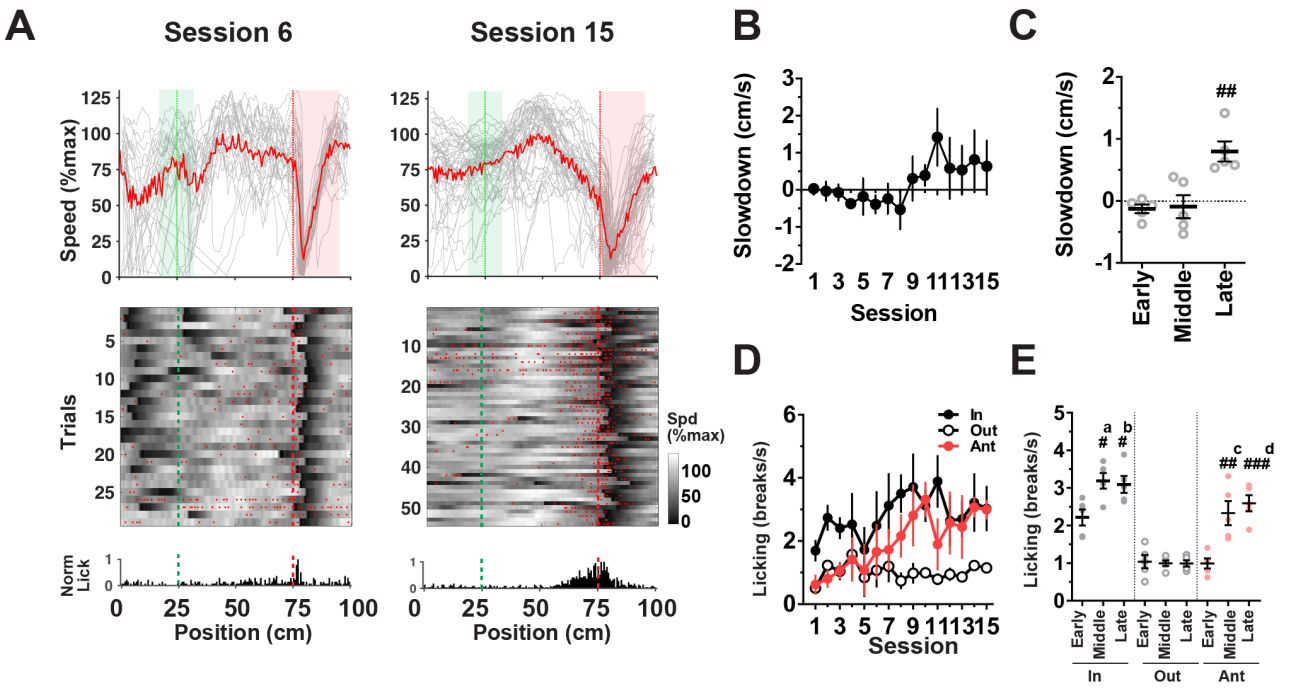

Figure S2. Training-induced increases in anticipatory slowdown and licking. Related to Figure 1. (A) Running speed and licking behavior of the same animal in session 6 (left) and session 15 (right). Average and trial-by-trial speeds against position are indicated in the top panels by the red and gray lines, respectively. In the middle panels, the speed for each trial is expressed in grayscale and is overlaid with licking, represented by red dots. The histograms in the bottom panels show normalized licking rates against position. The green and red dashed lines delineate the positions of the landmark and reward delivery, respectively. The areas shown in green and red define gate cells and reward cells, respectively (see Figure 2D). (B) Slowdown of running speed before the reward zone across sessions. n = 10 mice. (C) Average slowdown in the early, middle and late phases of training. $^{\#\#}P = 0.0017$ vs. Early, $F_{(2,12)} = 12.42$; one-way ANOVA, n = 5 sessions each (D) Licking rates within the reward zone (In, 75-95 cm from the origin), immediately before the reward zone (Ant, 65-75 cm from the origin) and elsewhere (Out) across sessions. n = 3 mice. (E) Average licking rates in the early, middle and late phases of training. $\#^{a}$, P = 0.016 vs. Early In, $\#^{b}$, P = 0.016 vs. Early In, $F_{(2,12)} = 6.12$; one-way ANOVA, n = 5 sessions each; $\#\#^{c}$, P = 0.0017 vs. Early Ant, $\#\#\#^{d}$, P = 0.0008 vs. Early Ant, $F_{(2,12)} = 13.4$; one-way ANOVA, n = 5 sessions each. Data in B–E are expressed as mean ± SEM.

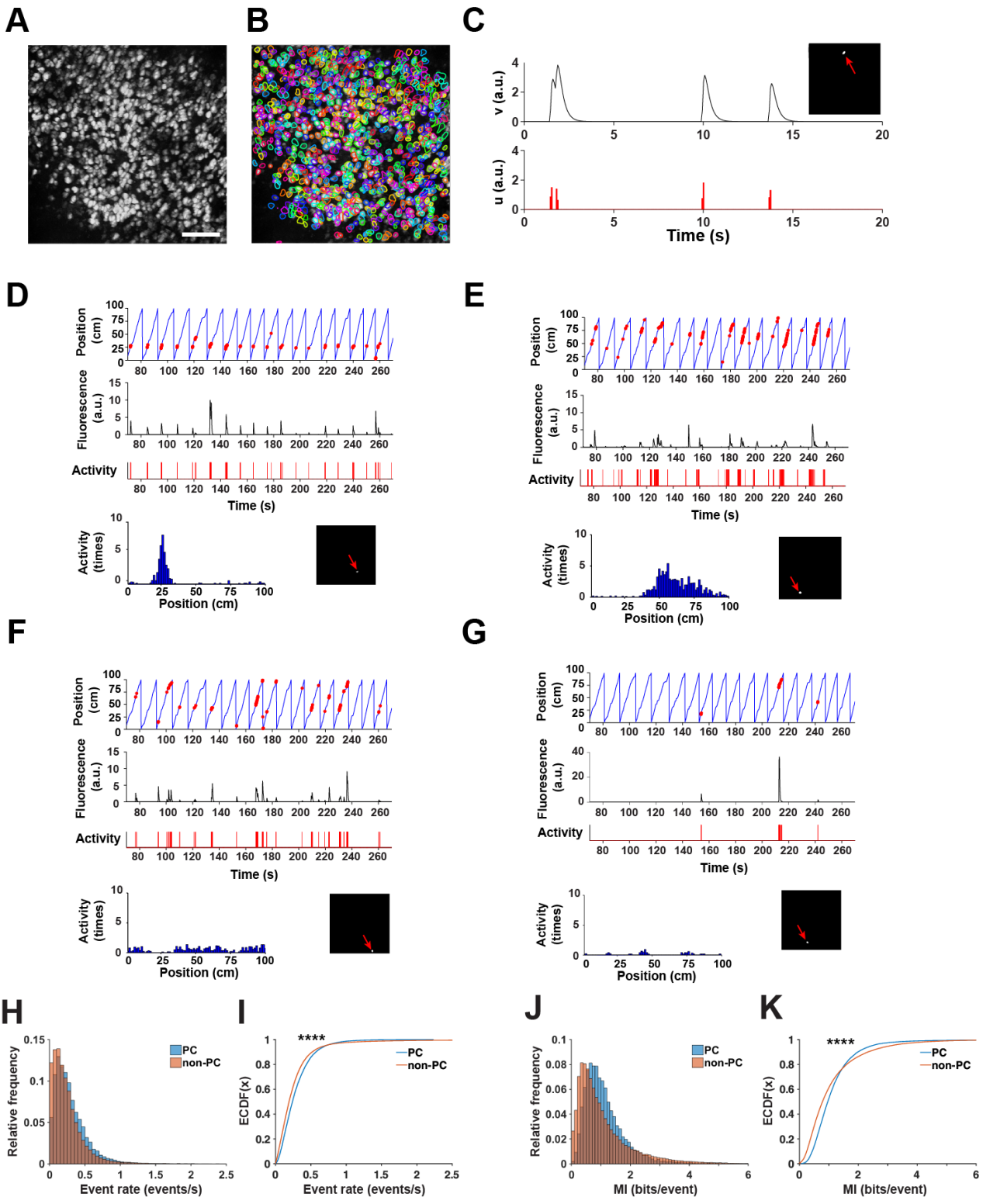
A
B
C
v (a.u.)
u (a.u.)
Time (s)
D
E
F
G
Position (cm)
Fluorescence (a.u.)
Activity
Time (s)
Activity (times)
Position (cm)
H
I
J
K
Relative frequency
Event rate (events/s)
ECDF(x)
MI (bits/event)
PC
non-PC
****

Figure S3. Spatiotemporal deconvolution of calcium imaging data and identification of place cells (PCs). Related to Figure 2. (A) A background-subtracted maximum intensity projection image that represents active cells in this example session. Scale bar = 100 μm. (B) Cell identification using the algorithm. In this session, 942 cells were identified. The contours of individual cells are shown by lines of different colors. (C) Time traces of fluorescence intensity (v, top) and inferred spike trains (u, bottom) of an example cell. The anatomical position of the cell is indicated by a red arrow in the inset. (D) Example of PCs. Shown from top to bottom are a time series of the mouse's virtual position with the timing of cellular activity indicated by red dots (top), a time series of fluorescence intensity (upper middle) and inferred cellular activity (lower middle), a histogram of cellular activity plotted against position on the virtual linear track (bottom left) and the anatomical position of the cell (bottom right). (E) Another example of PCs. This cell was imaged in a different part of the same field of view as D and activated at a different location on the virtual linear track. (F-G) Examples of non-PCs imaged in the same field of view as D and E. (H-I) Normalized histograms (H) and empirical cumulative distribution functions (ECDFs, I) showing the distribution of activity event rates of PCs (blue) and non-PCs (orange). ****$P < 0.0001$; PCs 0.29 ± 0.22 (event/s) vs. non-PCs 0.27 ± 0.35 (event/s), mean ± SD, n = 18,946 PCs and 75,563 non-PCs from 7 mice, two-sample Kolmogorov-Smirnov test. (J-K) Normalized histograms (J) and ECDFs (K) showing the distribution of mutual information content (MI) of PCs (blue) and non-PCs (orange). ****$P < 0.0001$; PCs 1.14 ± 0.85 (bits/event) vs. non-PCs 1.09 ± 1.02 (bits/event); mean ± SD, n = 18,946 PCs and 75,563 non-PCs from 7 mice, two-sample Kolmogorov-Smirnov test.

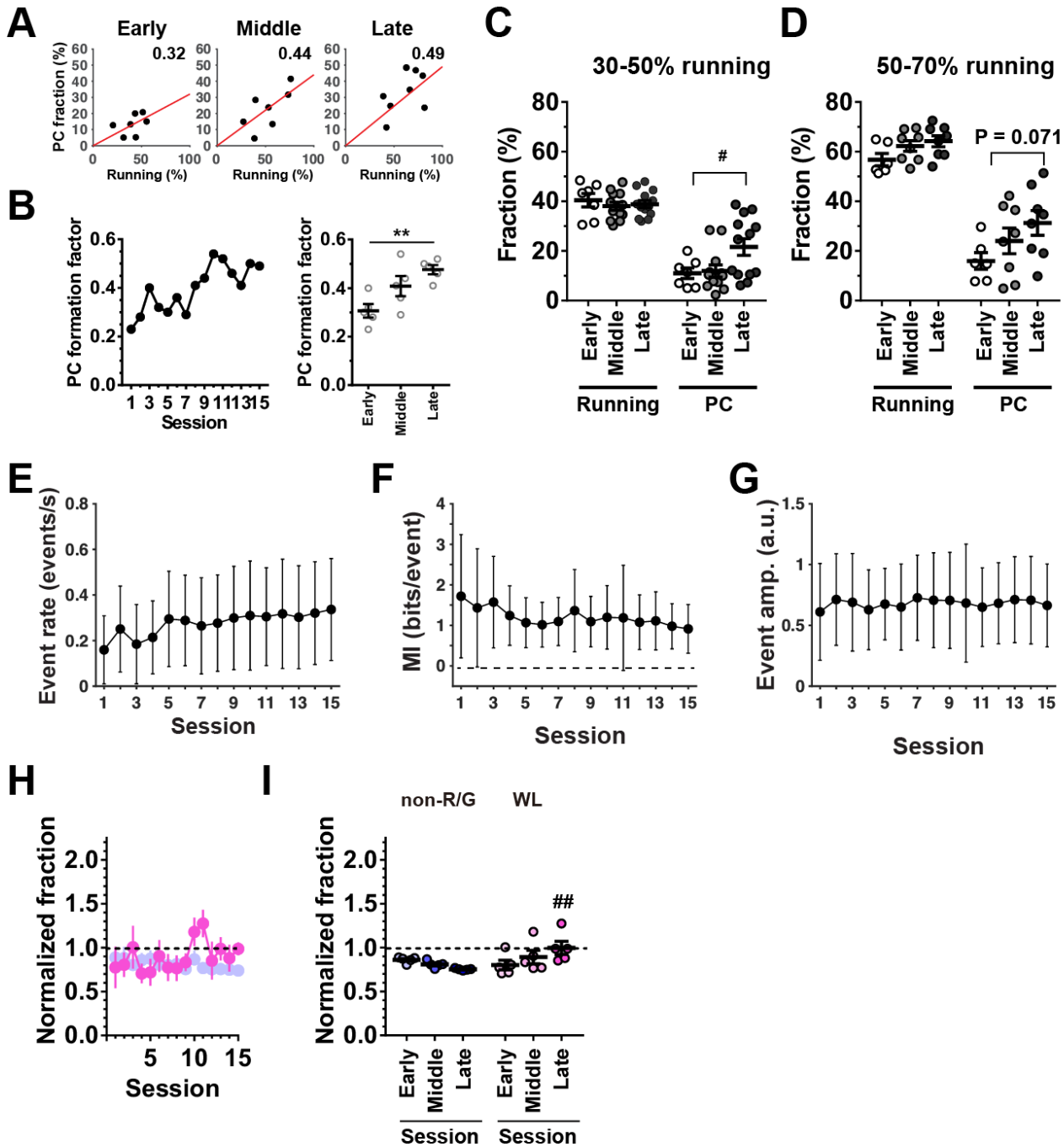
A
Early
Middle
Late
0.32
0.44
0.49
PC fraction (%)
Running (%)
B
PC formation factor
Session
**
C
30-50% running
Fraction (%)
#
Early
Middle
Late
Running
PC
D
50-70% running
P = 0.071
E
Event rate (events/s)
Session
F
MI (bits/event)
Session
G
Event amp. (a.u.)
Session
H
Normalized fraction
Session
I
non-R/G
WL
Normalized fraction
##
Session
Session

Figure S4. Training-induced increases in PC fractions and a delayed increase in PCs that encode a location of a boundary between different wall patterns. Related to Figure 2. (A) Example scatter plots showing the relationship between the fraction of PCs and the fraction of time spent running for the early (session 4), middle (session 9) and late (session 15) phases of training. The red line in each panel represents linear regression. The value shown at top right indicates the PC formation factor, which is defined as the slope of the regression line. (B) Changes of PC formation factors during training (left) and averages of PC formation factors for the early (sessions 1–5), middle (sessions 6–10) and late (sessions 11–15) phases of training (right). **P = 0.0022, $F_{(2,12)}$ = 7.64, ANOVA with post hoc test for linear trend, mean ± SEM, n = 5 sessions each. (C, D) Plots indicating mean fractions of time spent running and those of PCs in the early, middle and late phases of training. The sessions in which mice ran 30-50% (C) and 50-70% (D) of the time were analyzed. $^{\#}$P = 0.047, $F_{(2,29)}$ = 4.07, n = 7, 12 and 13 sessions, one-way ANOVA. The comparison between Early PC and Late PC in 50-70% running exhibited a near-significant trend (P = 0.071, $F_{(2,19)}$ = 2.55, n = 6, 8 and 8 sessions). Data are expressed as mean ± SEM. (E-G) Event rate (E), mutual information content (MI) (F), and event amplitude (G) of PCs across training sessions. Data are presented as mean ± SD (n = 428–2094 cells). (H) The fractions of wall cells (magenta) in each session are expressed as normalized fractions relative to a uniform distribution of PCs. The data on non-RW/GT cells in Figure 2E are presented again in this plot for comparison (blue). (I) Average normalized fractions of wall cells (WL) for the early, middle and late phases of training. The data on non-RW/GT cells in Figure 2F are presented again in this graph for comparison (blue). $^{\#\#}$P = 0.0079 vs. Late non-R/G, $U_{(5,5)}$ = 0, n = 5 sessions each, two-tailed Mann-Whitney test. Data in H and I are expressed as mean ± SEM.

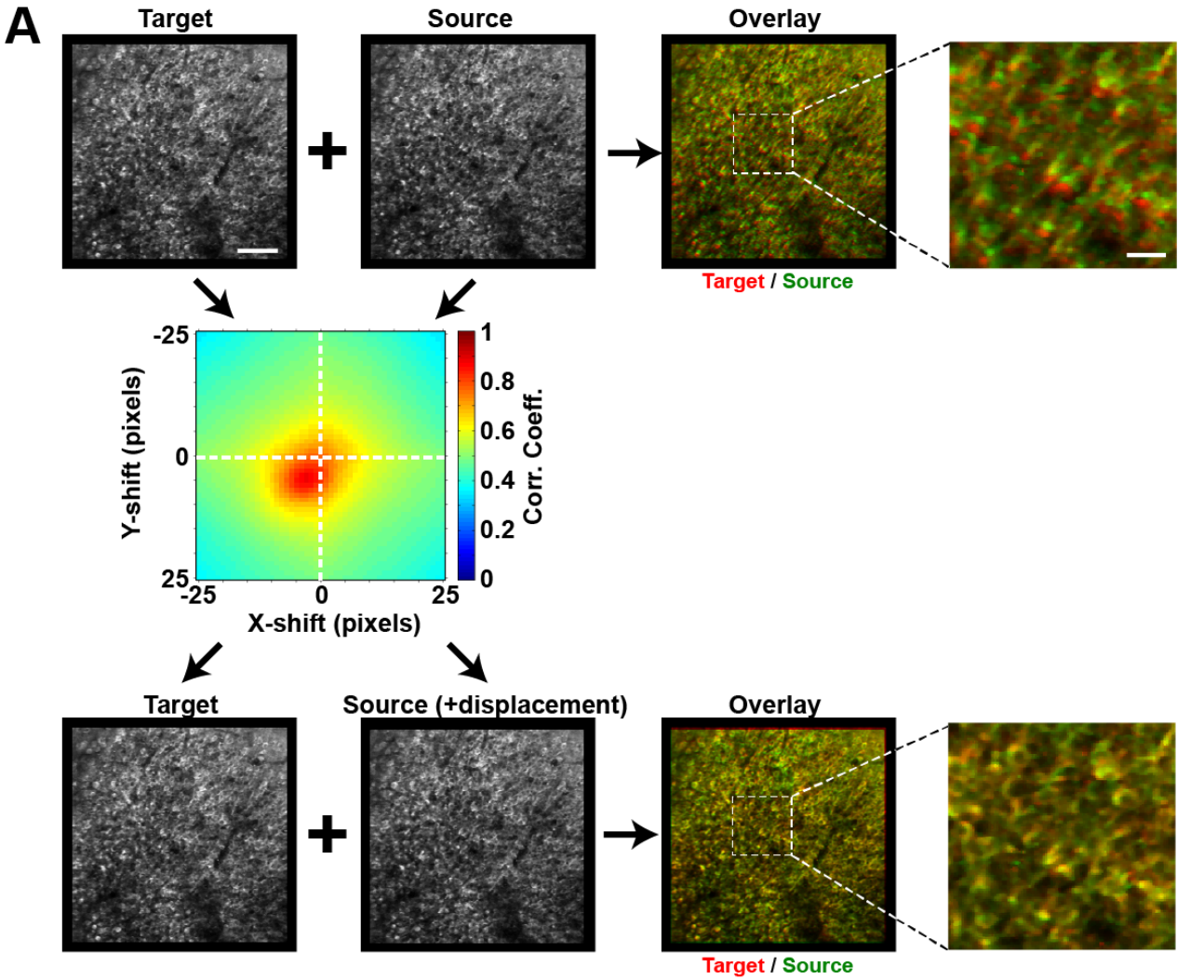
A
Target
Source
Overlay
Target / Source
-25
0
25
Y-shift (pixels)
X-shift (pixels)
1
0.8
0.6
0.4
0.2
0
Corr. Coeff.
Target
Source (+displacement)
Overlay
Target / Source

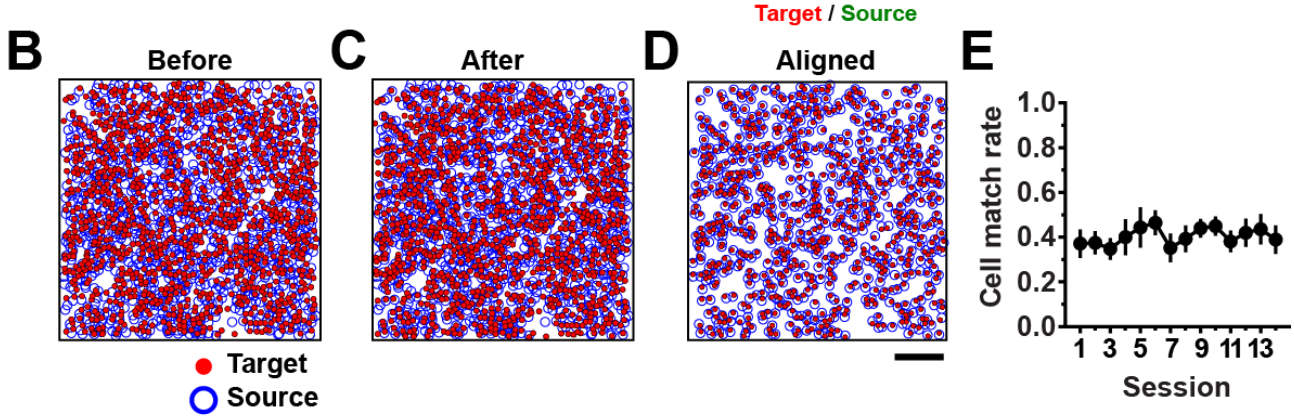
B
Before
C
After
D
Aligned
Target
Source

E
Cell match rate
1.0
0.8
0.6
0.4
0.2
0.0
1 3 5 7 9 11 13
Session

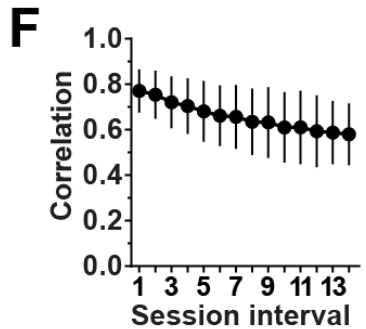
F
Correlation
1.0
0.8
0.6
0.4
0.2
0.0
1 3 5 7 9 11 13
Session interval

Figure S5. Alignment of cells across sessions. Related to Figure 3 and STAR Methods. (A) Image registration with or without the displacement estimated by two-dimensional correlation coefficients. A DsRed2 reference image of the target session (top left, scale bar = 100 μm) was overlaid with that of the source session (top center) without image displacement (top right, scale bar in magnified image = 25 μm). This placement resulted in global misalignment of cell positions between the target (red) and source (green) images. To correct this misalignment, two-dimensional correlation coefficients between the two images were calculated within a range of ± 25 × ± 25 pixel displacements (middle). The DsRed2 image of the same target session (bottom left) was then overlaid with that of the source session (bottom center) shifted by the amount of displacement that provided the maximum correlation coefficient (bottom right). This procedure improved global image alignment, as shown by an increase in well-aligned pixels, represented in yellow in the overlaid image. (B) Cells overlaid without correcting image displacement. Cells in the target and source sessions are presented as red dots and blue circles, respectively. (C) Cell aligned after the correction of image displacement. Many cells in both images are now properly aligned, and their local anatomical arrangements are mostly preserved. (D) Cell pairs that were considered to be the same cells are shown (see STAR Methods for detailed criteria). Scale bar = 100 μm. (E) The average fractions of cells aligned between two consecutive sessions. Values are expressed relative to the number of total cells identified in the target sessions (mean ± SEM, n = 7 mice). The X-axis indicates the earlier of the two sessions that were compared. (F) The average two-dimensional correlation coefficients plotted against the session intervals between the two images compared. Data are presented as mean ± SD (n = 7–98 session pairs).

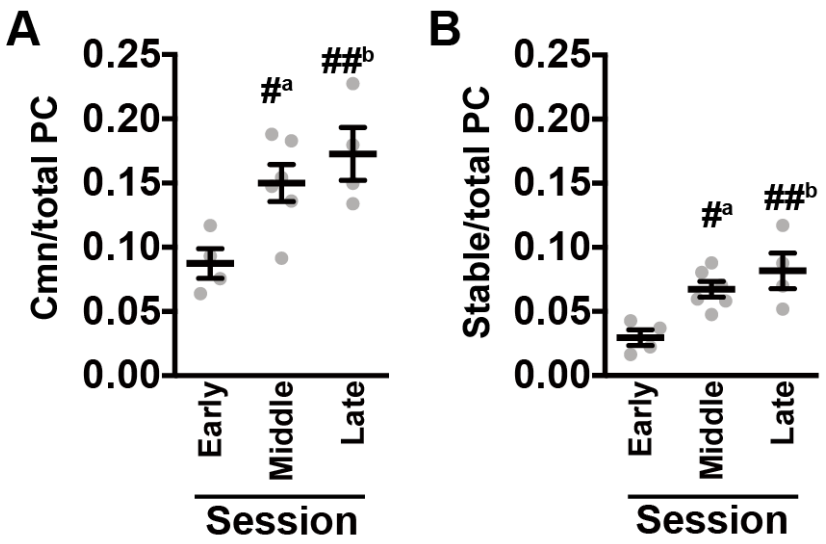

Figure S6. The experience-dependent increase in PC stability is not due to the increased number of PCs. Related to Figure 3. (A) Average fractions of common PCs relative to the number of total PCs for the early, middle and late phases of training. #[a], P = 0.029 vs. Early, ##[b], P = 0.0087 vs. Early, $F_{(2,11)} = 6.82$; one-way ANOVA, n = 4, 6 and 4 session pairs. (B) Average fractions of stable PCs relative to the number of total PCs. #[a], P = 0.019 vs. Early, ##[b], P = 0.0047 vs. Early, $F_{(2,11)} = 8.26$; one-way ANOVA, n = 4, 6 and 4 session pairs. Data are expressed as mean ± SEM.

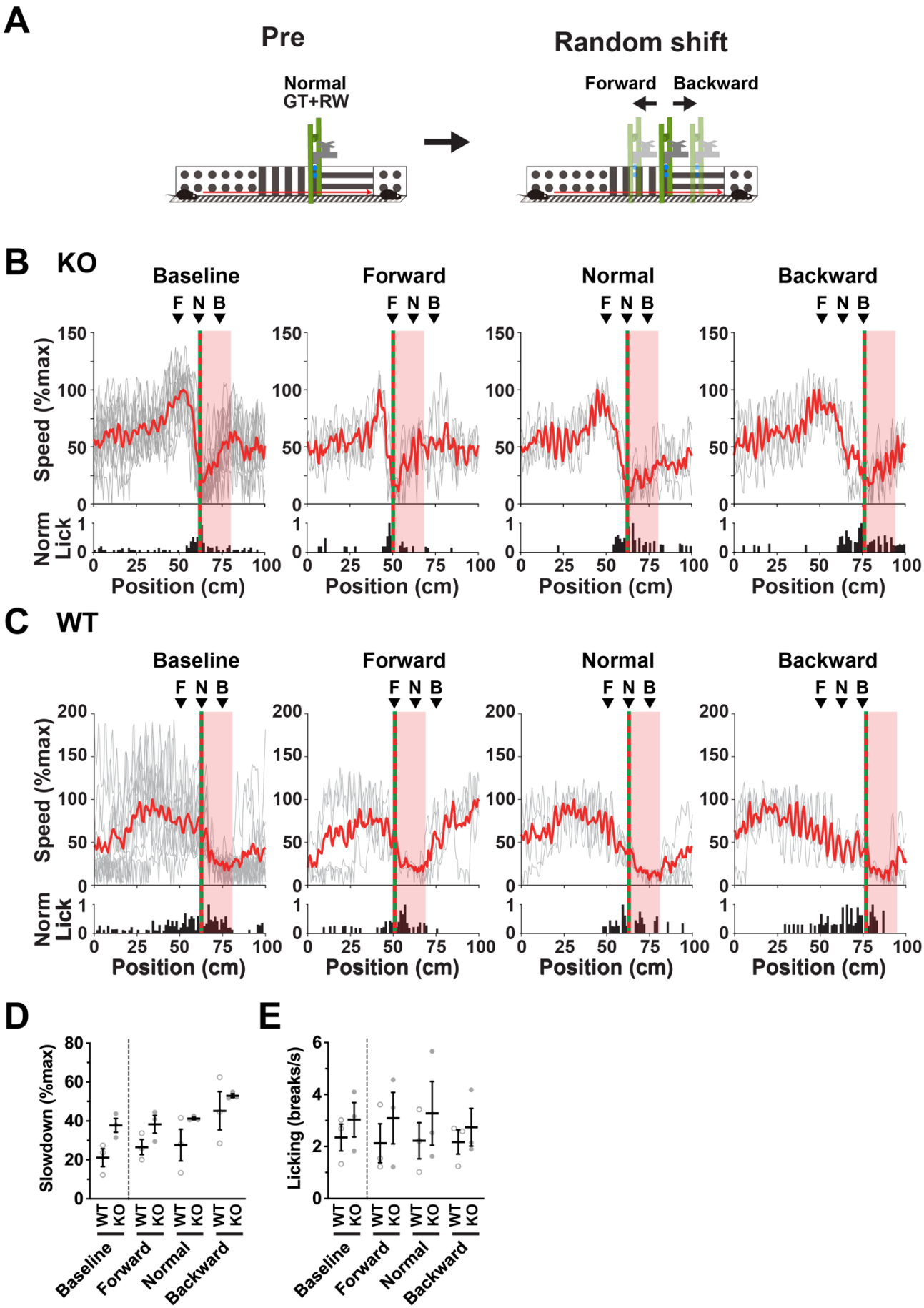
A
Pre
Random shift
Normal
GT+RW
Forward
Backward
B KO
Baseline
Forward
Normal
Backward
F N B
Speed (%max)
Norm Lick
Position (cm)
C WT
D
Slowdown (%max)
E
Licking (breaks/s)
WT
KO
Baseline
Forward
Normal
Backward

Figure S7. Visual recognition of the landmark is not impaired in Shank2-deficient mice. Related to Figure 7. (A) Design of the random gate shift task. Mice were pre-trained on the virtual linear track in which the visual landmark (GT) indicated the reward delivery point (RW; Pre, left). The following random shift sessions began with 12 baseline trials in which the GT + RW position was kept at the fixed location, followed by random shift trials in which their position was randomly shifted forward or backward or remained at the original position on a trial-by-trial basis (Random shift, right). The data for baseline, forward, normal and backward trials were analyzed separately. (B, C) Running speed and licking of Shank2-deficient mice (B, KO) and wild-type mice (C, WT) in representative sessions of the random gate shift task. The average and trial-by-trial speeds against position are indicated in the top panels by the red and gray lines, respectively. The histograms in the bottom panels show normalized licking rates against position. The lines in the alternate green and red colors represent the positions of GT + RW. The areas shown in red delineate the reward zone. F, N, and B represent the GT + RW positions in the forward shift, normal, and backward shift conditions, respectively. (D) Average slowdown of WT mice and KO mice in baseline, forward, normal and backward trials. (E) Licking rates of WT mice and KO mice immediately before the GT + RW position in baseline, forward, normal and backward shift trials. n = 3 WT mice and 3 KO mice. Data in D and E are expressed as mean ± SEM.